

Development of the Top Hat Electric Propulsion Plume Analyzer (TOPAZ): Mass Analyzer Design and Preliminary Calibration Data

IEPC-2005-016

*Presented at the 29th International Electric Propulsion Conference, Princeton University,
October 31 – November 4, 2005*

Allen L. Victor* and Thomas Zurbuchen†
University of Michigan, Ann Arbor, Michigan, 48109, USA

Alec D. Gallimore‡
University of Michigan, Ann Arbor, Michigan, 48109, USA

The continued development and testing of the Top Hat Electric Propulsion Plume Analyzer (TOPAZ) is presented for high-powered electric propulsion far-field plume diagnostics. TOPAZ incorporates a ‘top hat’ design with an analyzer constant of 100 resulting in a wide energy range and a high energy resolution. The design of the electrostatic and mass analyzer sections for TOPAZ is described. The key performance parameters for the analyzer are compared with theory, and preliminary mass-per-charge measurements on an ion beam are presented. A time-of-flight (TOF) system is incorporated into TOPAZ, and in conjunction with the energy analyzer section, provide a partial velocity distribution function measurement capability.

Nomenclature

E	=	particle energy
K	=	analyzer constant
R_1	=	deflection plate gap radius
R_2	=	grounded plate gap radius
R_3	=	top hat radius
R_C	=	gap centerline radius
R_G	=	guiding plate radius
R_p	=	particle radius of motion
S	=	aperture radius
V_D	=	deflection plate voltage
d_{gate}	=	gate distance
d_{TOF}	=	time-of-flight distance
m	=	particle mass
q	=	charge of particle
t_{TOF}	=	particle time-of-flight
u	=	particle velocity
ΔR	=	gap distance
Δx	=	distance between exit of gap and particle detector

* Graduate Student, Department of Aerospace Engineering, victora@umich.edu.

† Research Scientist, Atmospheric, Oceanic, and Space Sciences Department, thomasz@umich.edu.

‡ Professor, Department of Aerospace Engineering, alec.gallimore@umich.edu.

- α = elevation angle
- β = azimuthal angle of incoming particles
- θ = aperture angle
- φ = electric potential

I. Introduction

ELECTRIC propulsion (EP) offers power-efficient, high specific impulse (I_{sp}) options for deep-space missions as well as station keeping, orbital transfer, and attitude control requirements for near-Earth spacecraft. Hall thrusters are a type of EP system that utilizes electric and magnetic fields to produce thrust. Electrons emitted by a cathode travel upstream towards a positively-charged anode. A magnetic field that is applied in the perpendicular direction of the electric field hinders electron motion and creates a closed electron drift region. Propellant (e.g., xenon or krypton) is injected at the anode of an annular discharge channel, and ionized through collisions with the electrons caught in the closed electron drift region. The magnetic field has very little effect on the relatively massive ions. The electric field, however, accelerates the ions downstream away from the anode producing thrust. Currently, mid-power Hall thrusters achieve specific impulses between 1500-2500 seconds and electrical power efficiencies between 50-60%.¹

Recent trends in Hall thruster research by the USAF and US industry have included the high-power (> 20 kW) regime.² NASA is sponsoring high-power / high- I_{sp} (10 kW / ≥ 2000 s) Hall thruster technology through the NASA Glenn Research Center (GRC).³ The NASA-457 Hall Thruster developed at GRC produced the highest power level and thrust (75 kW and 2.9 N) achieved by any xenon-propellant Hall Thruster.⁴ High I_{sp} anode layer type (TAL) Hall thrusters have achieved specific impulses above 4100 s at this center as well.⁵

For these high-powered engines and future even more powerful engines being developed, plume characterization is imperative for determining their effect on spacecraft systems. Plasma transport properties, ionic charge state, and ion energy distributions are also important for understanding how Hall thrusters work and for improving their performance.⁶

One technique for determining the energy-to-charge distribution of plasma is to use an electrostatic analyzer. A specific geometry for the electrostatic analyzer, which allows for a wide field-of-view, is the top hat analyzer. This electrostatic analyzer consists of a sphere and a concentric shell with an aperture at the apex of the outer shell. The inner sphere is set to a specific voltage to allow for a narrow energy band of particles to pass through the aperture. By virtue of its geometry, the top hat analyzer is capable of having a 360-degree azimuthal field-of-view. Steering electric fields above the aperture allow for a field-of-view in the vertical direction as well. Structural constraints, however, diminish the total field-of-view in both directions.

The mass-per-charge of ions can also be determined through several methods. Magnetic sectors, quadrupole mass filters, and time-of-flight mass spectrometers are common techniques employed to determine the mass distribution of charged particles. TOPAZ incorporates a time-of-flight design to reveal the mass-per-charge spectrum of the plasma of interest.

The motivation for the design of the Top Hat Electric Propulsion Plume Analyzer (TOPAZ) is first discussed. The theory of operation for the energy analyzer and time-of-flight mass spectrometer is described, and the relevant design parameters are derived and related to the performance of the instrument.

II. Design Motivation

Electrostatic analyzers have been and are currently employed on spacecraft to investigate space plasmas such as solar wind as well as the ionospheres and magnetospheres of Earth and other planets.^{7,8} Space plasmas offer a wide range of particle energies from less than 1 eV to several MeV. This has led to design of electrostatic analyzers capable of detecting particles over several orders of magnitude in energy⁷; however, these types of plasmas have an ion number density several orders of magnitude lower than Hall thruster and ion engine plume.

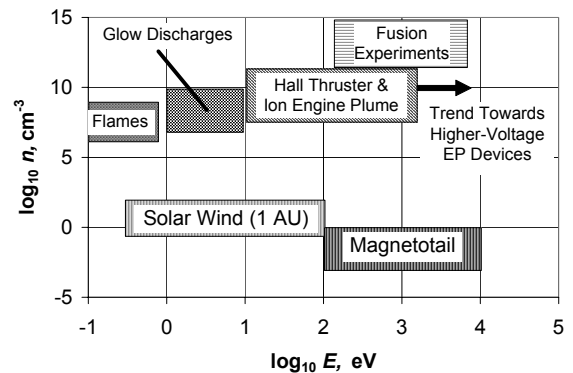


Figure 1. Number density and energy of typical space, laboratory, and electric propulsion plasmas.^{7,9,10}

Figure 1 describes the typical energy and number density ranges of space, laboratory, and Hall thruster and ion engine plasmas. The Hall thruster plume, the plasma of interest for TOPAZ, is nestled between laboratory plasmas (glow discharges and fusion experiments) and space plasmas (solar wind and the magnetotail) on the density scale. The energy range between Hall thruster plume and magnetotail plasma are similar. The primary difference between these two plasmas is the number density for the Hall thruster plume is several orders of magnitude greater.

There are many examples space plasma diagnostics through top hat analyzers. EP plume measurements with this type of device, however, are much rarer. The Plasma Experiment for Planetary Exploration (PEPE), flown on Deep Space 1 (DS1), included a dual top hat analyzer used to measure electrons and ions from the solar wind, spacecraft photoelectron sheath, and products of the xenon ion propulsion system. Low-energy xenon ions (< 40 eV) created from the beam ion interaction with neutral xenon particles were observed by PEPE.¹¹

Although beam ions were not measured by PEPE due to the position and orientation of the thruster with respect to the instrument, the observation of charge-exchange ions provides evidence for the top hat analyzer as a plume diagnostics tool for measuring facility effects. Hall thrusters have been shown to yield higher current density profiles in the far-field plume at higher background pressures. It is theorized that charge-exchange ions created from beam ions and neutral background particles are the culprit for the elevated current densities.¹² Diagnostic tools capable of characterizing the low energy charge-exchange ions as well as the high energy beam ions are therefore necessary to distinguish facility effects on plume diagnostics.

Charge states of propellant ions affect the charge-utilization efficiency, and hence the overall performance of Hall thrusters.¹³ An accurate measurement of the presence of multiple-charge states of propellant ions through a mass analyzer will provide an in-situ estimation of the charge-utilization efficiency. The time-of-flight technique utilized by TOPAZ for mass spectroscopy is presented in this paper.

III. Analyzer Design

The TOPAZ design theory is discussed in the following section. The design requirements for the analyzer are first described. SIMION, an ion trajectory code, was used to predict the angular and energy resolutions for TOPAZ. The final design for the analyzer was determined through an iterative process with SIMION. This is described in more detail in Ref. 14.

A. Design Requirements

An increase in power is expected for EP thruster development, and the acceleration potentials (and hence beam ion energies) are expected to increase in the foreseeable future. While Hall thruster voltages are not expected to increase above 2 keV, ion thrusters that are being considered for deep-space missions may have xenon ion beams of energy above 6 keV¹⁵. A Xe^{2+} ion would accelerate to 12 - 14 keV at this potential; hence TOPAZ has been designed to have a high energy measurement capability up to 15 keV. The nature of a top hat analyzer allows for the lower bound to be close to 0 eV, since the plate potentials correspond directly with the measured energy. The lower energy bound therefore is set by the accuracy of the power supplies used.

Since TOPAZ is a far-field plume diagnostics instrument, an adequate field of view of the thruster is required to "image" the ions projected from the entire discharge channel. A 30° vertical field-of-view allows for 57.7 cm of an object to be viewed from 1 m away, well within the size range of most thrusters. The azimuthal field-of-view is ideally 360° , but structural constraints diminish this to 112° . The angular resolutions of the field of view are within $2^\circ \times 2^\circ$ for the vertical and azimuthal directions, respectively. This resolution provides enough accuracy to determine a detected ion from the discharge channel, a different part of the thruster, or from the plume.

An adequate mass-per-charge resolution of TOPAZ is desired for detecting multiple-charge states (up to 4+) of propellants (e.g., Xenon and Krypton) and background ions in the chamber (e.g., N^+ and O^+). This allows TOPAZ to directly measure the charge-utilization efficiency of the thruster, as well as characterize the ingestion of background particles by the thruster inducing facility effects.

B. Theory of Operation

1. Electrostatic Energy Analysis

The top hat analyzer utilizes a radial electric field to guide ions through a spherical shell-shaped channel between a grounded plate and a negatively charged deflection plate. Figure 2 displays the key dimensions and plates for a top hat analyzer. The most important criterion is the ratio of the channel radius R_C to the gap distance ΔR ($\Delta R = R_2 - R_1$) which sets the analyzer constant (Eq. 1).

$$K \equiv \frac{R_C}{\Delta R} \quad (1)$$

The analyzer constant K determines the energy resolution, energy-to-voltage ratio, and other properties of the analyzer. The channel radius is simply the average of the inner and outer radii for the gap. Equating the applied force required to turn a particle at the channel radius with the electric field generated in the gap, the voltage is related to the energy-to-charge ratio. For high analyzer constants, the electric field can be assumed to be linear between the deflection plate and grounded plate. Equation (2) displays the simple relationship between the deflection plate voltage V_D , the analyzer constant, and the expected energy-to-charge ratio to be measured.

$$\frac{E}{q} = -\frac{KV_D}{2} \quad (2)$$

The top hat radius R_3 and the aperture angle θ determine the average elevation angle and the effective aperture area for the measured ions, respectively. The maximum ratio of detectable ions to incoming ions is realized when the top hat radius R_3 is at least as large as the analyzer gap distance.¹⁶ This ratio yields a top hat radius of approximately $R_3 = R_I + 2\Delta$.

The inner deflection plate radius R_I is held to a negative plate potential to detect positively charged ions. The outer radius is kept at ground potential. The top hat plate is also usually held at ground, but can be biased to increase transmissivity, or used as a gating plate for time-of-flight applications.

Guiding plates, which can vary either positively or negatively in plate potential, allow for variance in the vertical angular direction (elevation angle) for the measured ions. Ions coming from the selected elevation angle are guided into the top hat region such that their entrance angle is approximately horizontal above the deflection plate.

Ideally, the aperture angle θ (in radians) is proportional to the inverse square root of the analyzer constant.¹⁶

$$\theta \approx \sqrt{\frac{1}{K}} \quad (3)$$

The top hat plate should have the same radius as the aperture, such that the field generated between the top hat and the deflection plate is half that of the field between the deflection and grounded plates. This scenario allows for an ion to follow a “grazing” trajectory with the grounded plate and arrive at the detector.

2. Time-of-Flight Mass Spectroscopy

Time-of-flight mass spectrometers utilize the principle that particles of different masses with the same energy E travel with different velocities inversely proportional to the square root of the mass (Eq. 4).

$$u = \sqrt{\frac{2E}{m}} \quad (4)$$

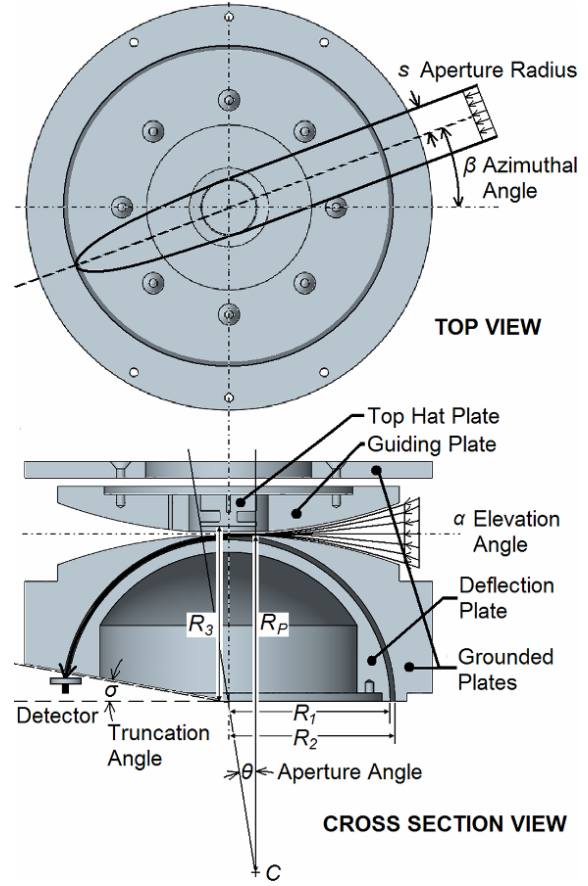


Figure 2. Principal design parameters of a top hat analyzer.¹¹

The time-of-flight t_{TOF} of the particle over a prescribed distance d_{TOF} is therefore directly proportional to the square root of the mass (Eq. 5).

$$t_{TOF} = d_{TOF} \sqrt{\frac{m}{2E}} \quad (5)$$

If the particle is an ion of charge q which has traveled over a potential $\Delta\phi$, Eq. (5) can be rewritten in terms of the mass-per-charge as a function of the time-of-flight (Eq. 6).

$$\frac{m}{q} = 2\Delta\phi \left(\frac{t_{TOF}}{d_{TOF}} \right)^2 \quad (6)$$

To determine the time-of-flight of a particle, the ions flow to the detector are turned “on” and “off” by use of the top hat plate which acts as an electrostatic gate. To “open” the gate, the top hat plate is biased with a positive voltage such that the transmission of ions through the channel to the detector is maximized. To “close”, the voltage of the plate is biased to a negative voltage (or ground if possible). In this state, no ions are able to travel through the aperture and arrive at the detector.

The use of the top hat plate as a gate for the ion flux to the detector requires voltage pulses, such that the pulse width is long enough for the slowest ion of interest to travel across the gate. However, if the gate is biased “on” for too long, a wider range of ions traveling at different velocities (i.e., different masses of the same energy) arrive at the detector at the same time. Therefore the smallest pulse width possible is desired to maintain the best mass resolution while not sacrificing a loss in signal from the slowest (and largest mass-per-charge) ion.

Equation (7) depicts the required pulse width t_{gate} required to allow the slowest ion to traverse across the gate distance d_{gate} .

$$t_{gate} > d_{gate} \sqrt{\frac{m_{max}}{2q\phi}} \quad (7)$$

The total distance the ion travels from the entrance of the gate (the leading edge of the aperture) to the detector is expressed in Eq. (8).

$$d_{TOF} = \frac{R_p\theta}{2} + \frac{\pi R_C}{4} + \Delta x \quad (8)$$

The first term represents the flight of the ion over radius R_p from the leading edge of the aperture entrance (see Fig. 2) to the centerline of TOPAZ over the middle of the aperture radius. The ion then travels through the channel at a radius of R_C making a 90° turn the entrance to the exit of the gap. Finally the distance between the exit of the gap and the entrance into the detector is represented as Δx .

For a time-of-flight analyzer, the ratio of the gate to the time-of-flight distance is related to the mass resolution (Eq. 9).¹⁷

$$\frac{d_{gate}}{d_{TOF}} \approx 1 - \sqrt{1 - \frac{\Delta m}{m}} \quad (9)$$

If the particle trajectory over the aperture is assumed to be approximately twice the channel radius R_C , Eq. (8) can be rewritten in terms of the analyzer constant K with help from Eq. (3).

$$d_{TOF} \approx \frac{R_C}{\sqrt{K}} + \frac{\pi R_C}{4} + \Delta x \quad (10)$$

All terms become non-dimensionalized by dividing Eq. (10) by the gate distance d_{gate} , which is approximately $R_C\theta$.

$$\frac{d_{TOF}}{d_{gate}} \approx 1 + \left(\frac{\pi}{4} + \frac{\Delta x}{R_C} \right) \sqrt{K} \approx 1 + \sqrt{K} \quad (11)$$

By relating Eq. (9) and Eq. (11), the mass resolution is shown to be inversely proportional to the analyzer constant to a first order approximation.

$$\frac{\Delta m}{m} \propto \frac{1}{K} \quad (12)$$

The above formulation indicates that top hat analyzers with high analyzer constants ($K > 50$) are particularly well-suited for time-of-flight techniques, since the ratio of the top hat plate (gate distance) to the channel distance (time-of-flight distance) is small.

C. Analyzer Design Specifications

Table 1 describes the design specifications and performance parameters for TOPAZ. A high analyzer constant of 100 was chosen to meet the energy resolution requirements. The high analyzer constant also aids in providing an adequate time-of-flight mass resolution. The angular resolutions and field-of-view were determined through SIMION and verified through experimental calibration. The method of the design and characterization of TOPAZ is discussed in further detail in a previous article.¹⁴

The biased and grounded plates in TOPAZ are made of Aluminum 6061-T6. High-temperature Machinable Glass Mica insulators are used to position the aluminum plates of TOPAZ in the correct position. Delrin, a non-conductive polymer (polyoxymethylene), provides the required separation for the top hat plate above the aperture.

Table 1. Physical and performance characteristics of TOPAZ.

PARAMETER	VALUE
Analyzer Constant, K	100
Inner Gap Radius, R_1	9.95 cm
Outer Gap Radius, R_2	10.05 cm
Gap Distance, ΔR	1 mm
Instrument Size (diameter)	24.6 cm
Geometric Factor, $G(E)$	$2.4 \times 10^{-5} \text{ cm}^2 \text{ sr eV/eV}$
Resolution ($\beta \times \alpha$)	$2^\circ \times 2^\circ$
Field-of-View ($\Delta\beta \times \Delta\alpha$)	$112^\circ \times 30^\circ$
Plate Material	Aluminum 6061-T6
Insulator Material	Delrin® and Glass Mica

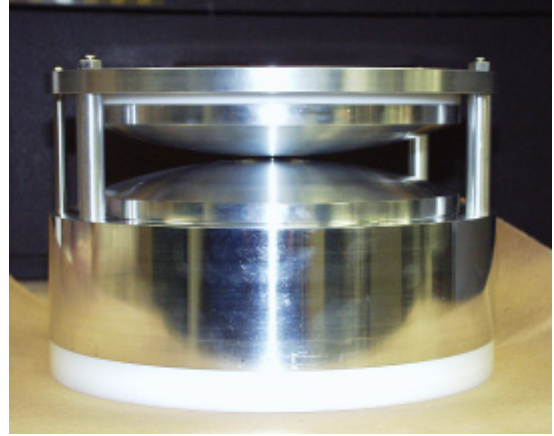


Figure 3. Final construction of TOPAZ.

IV. Calibration of the Time-of-Flight Mass Spectrometer

To verify the operation of the time-of-flight analyzer, TOPAZ was placed two meters downstream of an ion beam provided by the Department of Atmospheric, Oceanic, and Space Sciences at the University of Michigan. Ions of known energy and composition were flown through TOPAZ to characterize the time-of-flight mass spectrometer.

A. Experimental Setup

The setup consists of an Ion Accelerator attached to a 200,000 cm³ cylindrical chamber capable of maintaining a base pressure of 10⁻⁶ Torr. The ion beam has an energy range from 500 eV to 30 keV with intensity up to 1.5 nA over a 2 cm diameter beam size (0.477 nA/cm²).

A channel electron multiplier (CEM) with an aperture diameter of 1.0 cm was used to detect the ions exiting from TOPAZ through the gap. The CEM detects ions by accelerating them into a highly emissive secondary electron surface. An avalanche effect is created where these electrons create more secondary electrons, and a measurable pulse is created. Figure 4 describes the electrical schematic and controlling instrument setup for testing the TOPAZ time-of-flight mass spectrometer.

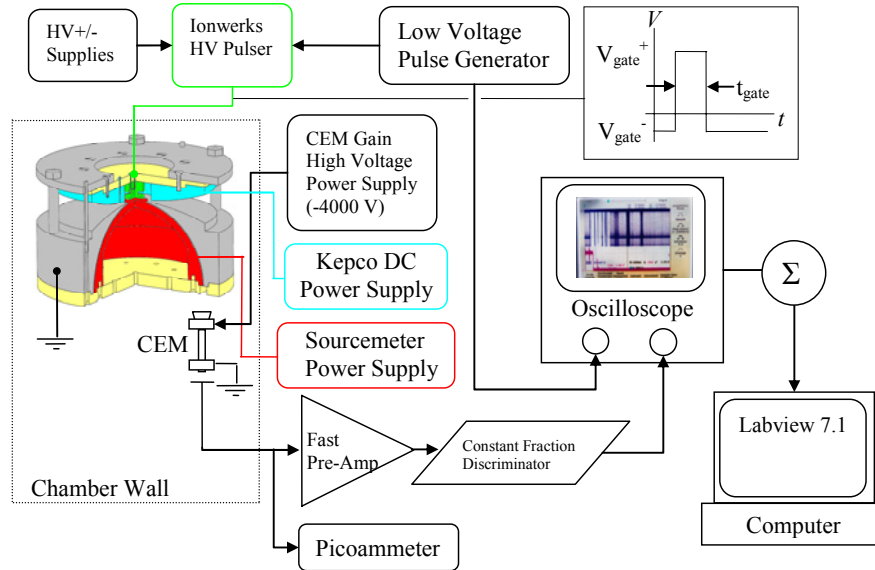


Figure 4. Electrical schematic of controlling electronics and data system for the time-of-flight mass spectrometer of TOPAZ.

The energy-per-charge of the ions detected by the CEM is determined by the voltage of the deflection plate (in red) set by the Sourcemeter power supply. The guiding plate potential (in turquoise) is controlled by a Kepco DC power supply. The voltage is set, such that the maximum number of ions fly through the aperture to be detected. The top hate plate potential (in green) is set by the Ionwerks High-Voltage Pulsar. A low voltage pulse generator sets drives the pulse width and frequency, while external high-voltage power supplies set the upper and lower peak voltages (V_{gate}^+ and V_{gate}^-). The pulse generator sends a signal to the oscilloscope for monitoring the start time of the pulse.

After an ion flies into the CEM, a pulse is created due to the avalanche of secondary electrons emitted. The gain for this response is controlled by a high-voltage power supply. The pulse exits the chamber, and the current is converted into a voltage pulse via the fast pre-amplifier. A constant fraction discriminator shapes the pulse such that the peak voltage and width are constant. The signal is sent to the oscilloscope, and the delay of detected ions with respect to the pulse generator is measured. The voltage as a function of time is summed over 2000 samples through Labview code and saved on a personal computer.

B. Experimental Procedure and Data

The ion beam energy was varied from 1 keV to 5 keV in 1 keV increments. Three gases were used as ion sources: krypton, xenon, and air. Krypton and xenon are common propellants used in Hall thrusters and ion engines. Air is composed of light gases, and therefore provided a challenging medium for time-of-flight measurements, since the velocities are much higher over the same energy range.

For all measurements, a “zero” profile is first taken with the deflection plate grounded. Spurious ions detected by the CEM, as well as transient signals generated by the pulser, are recorded and subtracted from measurements of

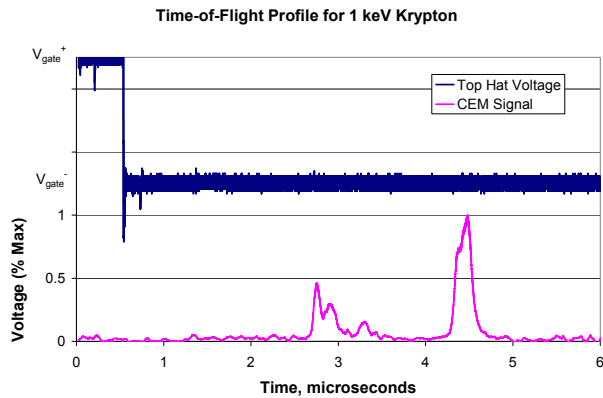


Figure 5. Sample voltage-time profile for a 1 keV krypton ion beam.

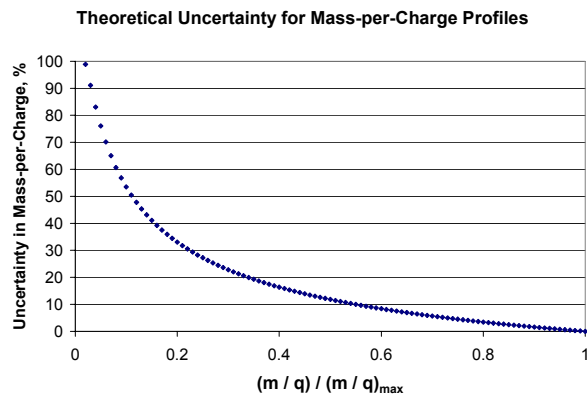


Figure 6. Theoretical uncertainty in mass-per-charge measurements.

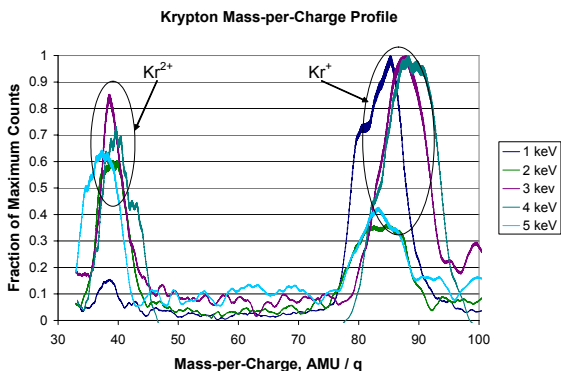


Figure 7. Mass-per-charge profile depicting singly and doubly charged Krypton for various beam energies.

profiles obtained for Krypton gas. The first and second charge states of krypton are easily identified for all beam energies in Fig. 7. The peak for the second charge stage of krypton is slightly shifted towards the left. This is due to the pulse width being larger than the time-of-flight for Kr^{2+} ions across the gate. The plots are calibrated such that

mass spectra with the deflection plate biased. Figure 5 displays a sample plot of the voltage profile generated for a 1 keV beam of krypton ions (summed over 2000 samples).

A boxcar average over 50 nanoseconds is performed over the CEM signal to smooth data and remove noise introduced by the cabling and picoammeter. This length in average was chosen since the peak detection and width were not significantly altered, while the noise variance was greatly reduced. Four peaks are noticeable from left to right corresponding with the Kr^{4+} , Kr^{3+} , Kr^{2+} , Kr^{1+} charge states, respectively. It is interesting to note, that the least voltage was received for the Kr^{2+} ion.

The delay in signal and the effective time-of-flight distance d_{TOF} are required to convert the voltage profiles into mass spectra. By correlating the peak arrival times measured and the theoretical time-of-flights for the different charge states of krypton, the delay in signal was found to be approximately 890 nanoseconds with a time-of-flight distance of 16.8 cm. The voltage measurements were converted into mass spectrum plots using this method for each species of gas.

The size of the pulse width determines the maximum mass-per-charge that will arrive to the detector. However, as the pulse width increases, the mass-per-charge resolution for lighter species decreases. Lighter ions have a larger window of opportunity through travel through the gate while it is “on,” since they have faster velocities. Ions with different mass-per-charges can arrive to the detector at the same time. This creates a broadening of peaks in the time-of-flight profiles. Although singly and doubly charged ions of heavy species (e.g., Kr^+ and Kr^{2+}) are readily discernable, the profiles of 3^+ and 4^+ charged heavy ions and lighter ions (e.g., Kr^{3+} , Kr^{4+} , N^+ , and O^+) become “blurred” together. There is an inherent uncertainty in the time-of-flight measurement for particles with mass-per-charges lower than the maximum permissible mass-per-charge through the gate. Figure 6 describes the relationship in uncertainty in mass-per-charge as a function of the maximum permissible mass-per-charge.

To alleviate the uncertainty in measuring mass-per-charge for light species and multiply charged propellant ions, a separate measurement was made with a smaller pulse width. The first measurements were optimized for singly and doubly charged heavy ions (with masses above 33 amu). A second set of measurements were done for masses below 33 amu. The pulse width was varied from 130 – 650 nanoseconds to obtain the most accurate measurement of the slowest moving ion species of interest in each profile.

Figure 7 and Fig. 8 describe the mass-per-charge profiles obtained for Krypton gas. The first and second charge states of krypton are easily identified for all beam energies in Fig. 7. The peak for the second charge stage of krypton is slightly shifted towards the left. This is due to the pulse width being larger than the time-of-flight for Kr^{2+} ions across the gate. The plots are calibrated such that

the singly charged ion peak is centered about the correct mass-per-charge. Doubly charged krypton ions, however, have an average earlier average arrival time, since the pulse width is larger than their time-of-flight across the gate. Therefore, the peak arrival time of ions arriving at the gate is earlier, and the mass-per-charge is calculated as being less than expected.

Figure 8 depicts the higher charge states of krypton and lighter elements measured. The third and fourth charge states of krypton are closer-spaced than the first and second, since the mass-per-charges are lower. The signal for the fourth charge state is higher than the third charge state in most cases. The most likely reason for this is the nonlinear gain provided by the CEM for higher energy ions. Peaks between 14 and 16 amu are noticed for some of the beam energies. This could represent background nitrogen and oxygen particles that have been accelerated through the ion beam. Below 5 amu, some of the measurements display possible hydrogen charge states. However, since the uncertainty in mass-per-charge is especially high for very light ions, this conclusion is taken with caution.

In Fig. 9 and Fig. 10, similar plots of the mass-per-charge for xenon are displayed. Figure 9 displays the single and double-charge states of xenon as principle peaks at approximately 131 amu and 65 amu, respectively. For the 2 keV xenon ion beam, anomalous peak is noticed at approximately 110 amu/q.

An attempt to discriminate the higher charge states of xenon was made; however, the noise overwhelmed the signal, and a clumping of the two charge states is observed. The noise below 20 amu is too significant to see peaks corresponding to nitrogen, oxygen, or lighter elements.

Since atmospheric elements are significantly lighter than propellant particles, a separate measurement of the mass-per-charge profile of air was conducted through the TOPAZ time-of-flight apparatus. Since air is composed mostly of nitrogen, calibration of the delay time in the signal and the pulse width were done assuming nitrogen as the primary element to be measured. Measurements of these lighter species proved challenging, since very short pulse widths were required to discriminate between lighter species.

Figure 11 displays the mass-per-charge profiles for air utilizing 2 keV to 5 keV beam energies. For beam energies 4 and 5 keV, the required pulse widths were 150 and 130 nanoseconds. Since this approaches the rise and fall times of the pulse generator (20 - 60 nanoseconds), the inaccuracy in the gating voltage is high, and a true "on" and "off" switch is not obtained over the aperture.

Peaks corresponding to the single charge states of nitrogen and oxygen are noticed, however peaks corresponding to multiple charge states (N^{2+} and O^{2+}) are absent. Measurements of hydrogen ions are coupled with noise, and it is unlikely particles with 3 - 5 amu are present in the chamber in significant quantities that could be detected by TOPAZ.

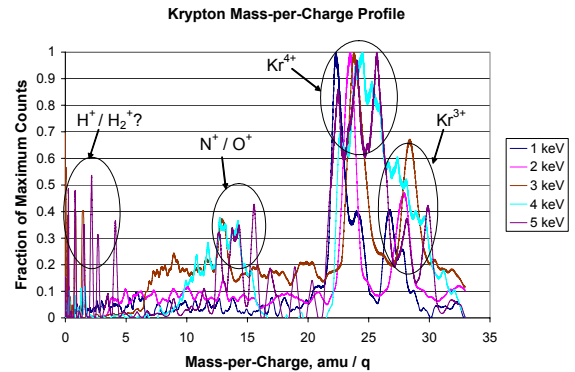


Figure 8. Mass-per-charge profile depicting multiply charged Krypton ions and lighter elements for various beam energies.

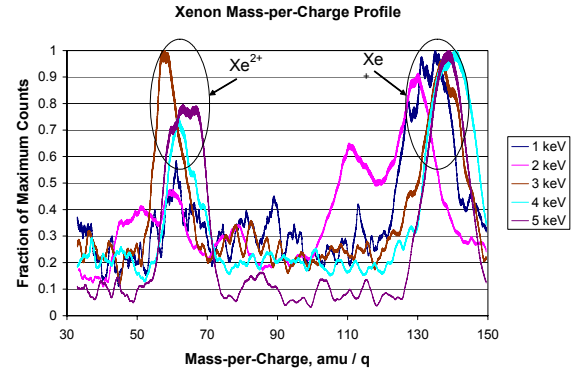


Figure 9. Mass-per-charge profile depicting singly and doubly charged Xenon for various beam energies.

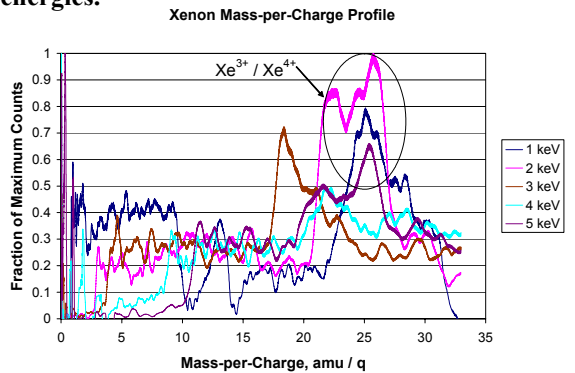


Figure 10. Mass-per-charge profile depicting multiply charged xenon ions.

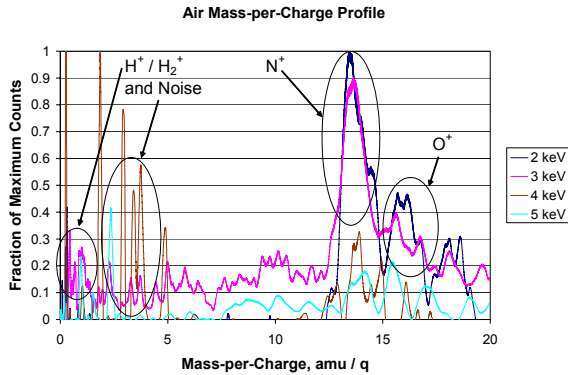


Figure 11. Mass-per-charge profile for air displaying nitrogen and oxygen ions at various beam energies.

Kr^{3+} . Since the CEM operates on an avalanche effect created from secondary electrons emitted by the first impact, the higher energy ions will generate more electrons, and hence a higher frequency pulse which is amplified by the fast-amplifier. In the calibration of the time-of-flight mass analyzer for TOPAZ, the number of counts generated by each species of ions was of little interest, and a very large CEM voltage of -4000 V was used to ensure a highly sensitive particle detector. For future measurements, where a measurement of the current fraction of each of charge-states of the propellant is desired, a lower CEM voltage (e.g., -1700 V) could be used while a larger sampling size (e.g., 10,000 instead of 2000) would compensate for the lower rate in particle detection.

Measurements on Xenon yielded easily discernable first- and second-charge states accelerated by the ion beam; however the third- and fourth-charge states are less defined than that of krypton. A possible cause for this is the use of a deflection plate voltage which is not exactly aligned with the ion beam energy for the xenon ion measurements. The ion beam energy fluctuates within a few percentages over the course of several minutes, due to the thermal load on the filament producing the ions. Since TOPAZ is highly sensitive to the energy-per-charge of ions detected due to its high energy resolution, the number of counts measured for the multiply-charged xenon ions could have decreased over the sampling. To alleviate the decrease in counts, a higher number of samples could be used to obtain a better representation of multiply-charge species of propellant ions.

The mass-per-charge profiles for both xenon and krypton confirm that time-of-flight mass spectrometry through TOPAZ is capable for detecting singly- and multiply-charged states for these propellants. Hall thrusters which utilize these propellants generate ions of similar charge-state at considerably lower energies (usually below 1 keV). Since lower energy particles offer longer time-of-flights and therefore use longer pulse widths which are more accurately obtained, the use of TOPAZ to determine ionic charge states of propellants in a Hall thruster plume is likely achievable.

The measurements of the ion beam utilizing air to generate the ionized particles indicate the discernment between nitrogen and oxygen is challenging but possible for energies between 2 – 3 keV. Above these beam energies, obtaining an accurate signal and providing a pulse voltage for the top hat plate with short pulse widths and step function voltages is difficult. The primary motivation for these measurements is to detect background chamber particles which have been ingested by an EP device and accelerated into the plume to generate artificial thrust (yielding facility effects). As with propellant ions, the energies these particles are accelerated by Hall thrusters and ion engines are significantly less than those measured with the ion beam. Therefore, TOPAZ is probably capable of detecting these particles in EP plumes and providing a qualitative measurement of facility effects on the thruster.

V. Discussion

Measurements on the krypton and xenon ion beams yield charge states similar to those obtained on Hall thrusters operating on the same propellants.¹⁸ For krypton the first two charge states are easily discernable for beam energies from 1–5 keV. The slight shift to the left for the doubly-charged krypton and xenon peaks (Fig. 7 and Fig. 9) is attributed to the optimization of the pulse width for the singly-charged species. A similar effect of peak-shifting is seen in the mass-per-charge profiles for the third and fourth charge states of krypton and xenon in Fig. 8 and Fig. 10.

Figure 8 depicts that the counts obtained for the fourth-charge state of krypton are significantly higher than the third-charge state. This is most likely due to the impact energy of the Kr^{4+} being significantly higher than

VI. Conclusions

Calibration of the TOPAZ time-of-flight mass spectrometer was conducted through use of an ion beam utilizing krypton, xenon, and air as ion sources. The first four charge-states of krypton were measured and three charge-states of xenon were detected for beam energies of 1 – 5 keV. Singly charged oxygen and nitrogen ions were also detected for energies of 2 – 3 keV. Hydrogen ions might have been measured, however the uncertainty in measurement for these high-velocity ions is significant, and the noise present is not discarded as a possible candidate for the peaks observed in the mass-per-charge profiles. The optimum pulse widths and characteristic time-of-flight distance was

determined for TOPAZ, and the analyzer has been qualified as a potential candidate for mass spectroscopy in far-field electric propulsion plumes.

Acknowledgments

The authors greatly acknowledge Dr. Stefan Scherer for his lease of the ion accelerator and vacuum chamber for the characterization of TOPAZ. The authors thank Chuck Navarre and Robb Gillespie for their highly precise machining of the parts. Finally, the authors thank Robert Lundgren for offering his expertise on the design and testing of the time-of-flight mass spectrometer. A. Victor is supported by the NASA-funded Michigan Space Grant Consortium as well as the Department of Aerospace Engineering at the University of Michigan.

References

- ¹Haas, J. M., Gulczinski, F. S., and Gallimore, A. D., "Performance Characteristics of a 5 kW Laboratory Hall Thruster," AIAA-97-3503, 34th Joint Propulsion Conference, Cleveland, OH, July 1998.
- ²Spores, R. A., Spanjers, G. G., Birkan, M., Lawrence, T. J., "Overview of the USAF Electric Propulsion Program," AIAA-2001-3225, 37th Joint Propulsion Conference, Salt Lake City, UT, July, 2001.
- ³Dunning, J., Sankovic, J., "NASA's Electric Propulsion Program," AIAA-2000-3145, 36th Joint Propulsion Conference, Huntsville, AL, July 2000.
- ⁴Manzella, D., Jankovsky, R., Hofer, R., "Laboratory Model 50 kW Hall Thruster," AIAA-2002-3676, 38th Joint Propulsion, Indianapolis, IN, July 2002.
- ⁵Jacobson, D. T., Jankovsky, R.S., Rawlin, V. K., Manzella, D. H., "High Voltage TAL Performance," AIAA-2001-3777, 37th Joint Propulsion Conference, Salt Lake City, UT, July 2001.
- ⁶Gallimore, A. D., "Near- and Far-Field Characterization of Stationary Plasma Thruster Plumes," *Journal of Spacecraft and Rockets*, Vol. 38, No.3, 2001, p. 441-453.
- ⁷Bame, S. J., McComas, D. J., Young, D. T., Belian, R. D., "Diagnostics of Space Plasmas," *Review of Scientific Instruments*, Vol. 57, No. 8, August 1986, p. 1711-1716.
- ⁸Vilppola, J. H., Tanskanen, P. J., Huomo, H., Barraclough, B. L., "Simulations of the Response Function of a Plasma Ion Beam Spectrometer for the Cassini Mission to Saturn," *Review of Scientific Instruments*, Vol 67, No. 4, April 1996, pp. 1494-1501.
- ⁹Hofer, R. R., Haas, J. M., Gallimore, A. D., "Ion Voltage Diagnostics in the Far-Field Plume of a High-Specific Impulse Hall Thruster," AIAA-2003-4556, 39th Joint Propulsion Conference, Huntsville, AL, July 20-23, 2003.
- ¹⁰Herman, D. A., Gallimore, A. D., "Comparison of Discharge Plasma Parameters in a 30-cm NSTAR Type Ion Engine with and without Beam Extraction," AIAA-2003-5162, 39th Joint Propulsion Conference, Huntsville, AL, July 20-23, 2003.
- ¹¹Young, D. T., Nordholt, J. E., Hanley, J. J., "Plasma Experiment for Planetary Exploration (PEPE) DS1 Technology Validation Report," JPL Publication 00-10, 2000.
- ¹²Walker, M. L. R., Hofer, R. R., Gallimore, A. D., "The Effects of Nude Faraday Probe Design and Vacuum Facility Backpressure on the Measured Ion Current Density Profile of Hall Thruster Plumes," AIAA-2002-4253, 38th Joint Propulsion Conference, Indianapolis, IN, July 7-10, 2002.
- ¹³Hofer, R. R., Gallimore, A. D., "Efficiency Analysis of a High-Specific Impulse Hall Thruster," AIAA-2004-3602, 40th Joint Propulsion Conference, Fort Lauderdale, FL, July 11-14, 2004.
- ¹⁴Victor, A. L., Zurbuchen, T. H., Gallimore, A. D., "Development of the Top Hat Electric Propulsion Plume Analyzer (TOPAZ)," AIAA-2004-4099, 40th Joint Propulsion Conference, Fort Lauderdale, FL, July 11-14, 2004.
- ¹⁵S. Oleson, "Electric Propulsion for Project Prometheus," AIAA-2003-5279, 39th AIAA/ASME/SAE/ASEE Joint Propulsion Conference and Exhibit, Huntsville, Alabama, July 20-23, 2003.
- ¹⁶Carlson, C. W., McFadden, J. P., "Design and Application of Imaging Plasma Instruments," *Measurements Techniques in Space Plasmas: Particles*, edited by R. F. Pfaff, J. E. Borovsky, and D. S. Young, AGU Geophysical monograph, Washington, DC, 1998, pp. 125-140.
- ¹⁷King, L. B., "Transport-property and Mass Spectral Measurements in the Plasma Exhaust Plume of a Hall-effect Space Propulsion System," Ph.D. Dissertation, University of Michigan, 1998.
- ¹⁸Linnell, J.A., Gallimore, A.D., "Efficiency Analysis of a Hall Thruster Operating with Krypton and Xenon," AIAA-2005-3683, 41st Joint Propulsion Conference, Tucson, AZ, July 10-13, 2005.